Observation of Strong Oscillations of Areal Mass in an Unsupported Shock Wave

Y. Aglitskiy, M. Karasik, A. L. Velikovich, V. Serlin, J. Weaver, T. J. Kessler, A. J. Schmitt, S. P. Obenschain, N. Metzler, and J. Oh

Phys. Rev. Lett. **109**, 085001 — Published 20 August 2012

DOI: 10.1103/PhysRevLett.109.085001

Observation of strong oscillations of areal mass in an unsupported shock wave

Y. Aglitskiy,[1] M. Karasik,[2] A. L. Velikovich,[2] V. Serlin,[2] J. Weaver,[2] T. J. Kessler,[2] A. J. Schmitt,[2] S. P. Obenschain,[2] N. Metzler,[3,4] and J. Oh[3]

[1]*Science Applications International Corporation, McLean, VA 22150*
[2]*Plasma Physics Division, Naval Research Laboratory, Washington, DC 20375*
[3]*Research Support Instruments, Lanham, MD 20706*
[4]*Ben Gurion University, Beer Sheva, Israel*

Experimental study of hydrodynamic perturbation evolution in a strong unsupported shock wave, which is immediately followed by an expansion wave, is reported. A planar solid plastic target rippled on the front side is irradiated with a 350-450 ps long laser pulse. The perturbation evolution in the target is observed using face-on monochromatic x-ray radiography during and for up to 4 ns after the laser pulse. The theoretically predicted large oscillations of the areal mass in the target are observed for the first time. Multiple phase reversals of the areal mass modulation are detected.

PACS numbers: 52.57.Fg, 52.70.La, 52.35.Tc, 47.20.Ma

About a decade ago direct-drive approach to laser fusion was based on capsule irradiation with a laser pulse that started with a lower-intensity foot, to set the accelerated fuel on the desired adiabat, followed by a gentle rise to the peak intensity maintained throughout the inward acceleration [1]. In recent years, advantages of direct-drive implosion scenarios that involve hitting the target with one or more short laser pulses, or spikes have been demonstrated. A spike, or sequence of several spikes, preceding the main pulse can not only substitute for the foot in setting the fuel on the desired adiabat, but can also tailor the spatial profile of the adiabat (i. e., make the adiabat high near the ablation front, thereby improving the target resistance to perturbation growth, while keeping it low in the fuel), see [2-5] and references therein. In the shock ignition scenario [6], a strong, short ignitor pulse irradiates the target after the driving pulse is over, sending a converging unsupported shock wave to the central hot spot to compress, heat and ignite it.

According to the traditional scenario of direct-drive laser fusion [1], the formation of the initial mass nonuniformities, which are later amplified by the Rayleigh-Taylor (RT) instability growth in the imploding target, takes place during the foot of the laser pulse, when the laser maintains a Mbar-range pressure in the target but before it starts accelerating. This early-time perturbation evolution has been studied in detail, in theory, simulation, and experiment, for all sources of initial non-uniformity (roughness of the outer and inner target surfaces, nonuniformities localized at imbedded interfaces, laser imprint) and all the hydrodynamic mechanisms of the RT seed formation, which include, but are not limited to, ablative Richtmyer-Meshkov (RM) instability [7-10] and feedout [11-13], see also [14-17] and references therein.

Much less is known about the evolution of perturbations in a target after a short, strong laser pulse. The energy deposited by the laser produces an unsupported, decaying shock wave, which propagates into the target immediately followed by an expansion wave. Theoretical and computational perturbation analysis for such combination of waves has been first performed in [18] for the case when the front surface of the target is rippled. Both the ripple amplitude of the shock front η_s and the areal mass modulation amplitude δm have been shown to experience very strong oscillations. The amplitude η_s has been shown to exceed the initial ripple amplitude η_0 by a factor of 2, whereas δm can exceed its initial value, $\delta m_0 = \rho_0 \eta_0$, by an order of magnitude. The oscillations of the coupled shock and rarefaction wave are amplified due to the mechanism identified for an isolated rarefaction wave [19].

Experimental observation of this effect is of general interest for compressible fluid dynamics. Unsupported shock flow is a response of a medium to a strong, short impact, revealing the "Green's function," the eigenfrequencies of the shocked target. The mechanism producing the unusually strong impact-generated oscillations *after* the impact has been studied theoretically and numerically in [18], but the effect, predicted to be observable in a rippled target hit with a short laser pulse, has never been observed before.

The basics of such an experiment are illustrated in Fig. 1. It shows the results of a simulation performed using the FAST2D hydrocode developed at the Naval Research Laboratory (NRL) [20] and validated against our extensive experimental data on ablative and classical RM instability [8, 10, 21]. All our simulations use inverse Bremsstrahlung absorption, classical Spitzer-Härm electron thermal conductivity (no flux limiter) and the NRL baseline CALEOS equation-of-state model [22] roughly equivalent to the quotidian

equation of state QEOS [23]. In the simulation of Fig. 1 plasma radiation was not taken into account. A pulse of krypton fluoride laser with wavelength $\lambda_L = 248$ nm, peak intensity 2.3×10^{14} W/cm^2, idealized Gaussian pulse shape (FWHM=350 ns, truncated at $t = \pm 0.5$ ns) propagating in the negative x direction is normally incident upon a 100 μm thick plastic target. The target has single-mode ripple pattern on the front surface (ripple wavevector in the y direction, wavelength $\lambda = 30$ μm, peak-to-valley amplitude $\eta_0 = 5$ μm). The propagation of the shock wave is visualized in Fig. 1(a) through the one-dimensional particle $x-t$ trajectories. The laser pulse ends at $t = 0.5$ ns, after which the slowing down of the unsupported shock wave is seen. The shock wave breaks out at the rear surface of the target at $t = 1.67$ ns.

Evolution of areal mass perturbations in the target is illustrated by Fig. 1(b). Here and below, the amplitude δm is normalized with respect to the initial target density, $\rho_0 = 1.07$ g/cm^3 and thereby shown in μm. Solid and dotted lines show, respectively, the areal mass modulation amplitude in the target whose thickness is 100 μm (thick target) and 53 μm (thin target). For the thin target, the shock front breaks out at its rear surface at $t = 0.6$ ns, shortly after the end of the laser pulse. Up to this moment, these two lines coincide, as they should. After that, the solid line corresponds to the propagation of an unsupported shock wave through the unperturbed part of the thick target, and the dotted line – to the perturbation evolution in a disintegrating thin target.

While the laser pulse lasts, we see the amplitude δm rise and fall. This first half-oscillation, caused by the ablative RM instability [7-10, 14-16], provides the initial conditions for the subsequent oscillations in the target illustrated by the pressure maps of Fig. 1(c). Lateral pressure gradient, whose prevailing direction is shown by the arrows,

accelerates the shocked mass that freely expands into vacuum along the x axis. The lateral mass flow continues when the lateral pressure gradient vanishes, thus overshooting the equilibrium situation and building up a reversed pressure gradient, cf. Fig. 1(c). When the mass starts moving in the reverse direction, the laterally averaged pressure decreases due to rarefaction compared to the pressure difference that originated the lateral flow. As a result, the oscillation amplitude does not decay as fast as in a supported shock wave; under certain conditions, which are not fulfilled in our experiments, it might even keep growing for some finite time. In hydrodynamics, an exact analogy of this process is the Vishniac instability of a blast wave in planar geometry [24].

Note how strong the simulated areal mass oscillations are. For comparison, recall the oscillations in a supported rippled shock wave that decay very rapidly from their initial amplitude (cf. Figs. 3(a), 4 of [25] and Fig. 4 of [16]). A rippled expansion wave propagating through a target where the pressure is supported by the laser, as in the feedout situation, when the rear surface of the target is rippled, also produces strong oscillations [19]. The experimental constraints, however, make it difficult to observe more than a quarter-period of such oscillations, as in [4, 13, 14]: once the head of the rippled rarefaction wave breaks out at the ablation front, the oscillations give way to monotonic RT growth [11]. Here, the strong oscillations occur since the end of the short spike, and, in the case of a 100 μm thickness, proceed while the unsupported shock wave propagates into the unperturbed target, and even some time after that.

Detailed experimental study of the predicted strong oscillations has become possible recently, when the capability to produce strong short pulses (FWHM 350-500 ps, peak intensity up to 3.3×10^{14} W/cm^2 in a Ø750 μm focal spot with a Ø400 μm flat top)

was added to the main drive beams of the Nike laser [26]. The monochromatic x-ray imaging system on Nike is based on Bragg reflection from spherically curved crystals [8, 10, 16, 27]. A silicon backlighter target is used to radiograph the main target for about 5 ns. A spherically curved quartz crystal selects the resonance line of He-like Si (1.86 keV) and projects a monochromatic image of the target on the slit of an x-ray streak camera. The monochromatic face-on x-ray imaging makes it possible to translate the observed modulation of the optical thickness directly into the modulation of the areal mass. The overall spatial resolution is characterized by the modulation transfer function, which for the 30 to 45 μm spatial wavelength was in the acceptable range of 0.55 to 0.65. The streak camera slit width of 500 μm was selected as a compromise to give sufficient time resolution (≈200 ps) to observe the phase reversals and retain the ~1 μm sensitivity for a 100 μm thick target.

We used laser machined polystyrene targets with single-mode ripple wavelengths of $\lambda = 30$ μm and 45 μm, and initial peak-to-valley amplitude in the range between 3 and 8 μm. Target thicknesses ranged between 53 and 125 μm. Thicker targets provide longer observation time of the oscillations before the shock breaks out on the rear and the target starts decompressing. The maximum allowable thickness of the target is limited by the corresponding signal loss at the streak camera due to the increased absorption of backlighting x-rays in the target.

The choice of the ripple wavelength was determined by the desire to observe several phase reversals during the shock transit (shorter perturbation wavelength gives shorter oscillation period) and the need to resolve the ripples with high fidelity. We used relatively large initial ripple amplitudes for the sake of tracking the mass perturbation

history from the initial time, before they grow. Even more important, such a choice gave us the ability to continue to see the phase reversals of the areal mass modulation δm even as its amplitude decays in time.

Such choice of initial amplitudes corresponds to the nonlinearity parameter $k\eta_0$ ranging between 0.6 and 1.1. Hence our initial amplitudes are not small and the observed oscillatory behavior is nonlinear. Because there is no exponential growth here and all of the processes involved in the perturbation evolution are oscillatory (both when the laser pulse is on and off), the mode determined by the initial ripple should dominate the perturbation evolution. We have, however, observed an appearance of the second spatial harmonic in some shots with target wavelengths of 30 μm and initial amplitude greater than 5 μm. For longer wavelength of 45 μm and amplitudes < 5 μm high harmonics effect appeared to be less significant.

Figure 2 compares the observed time evolution of the areal mass modulation amplitude δm for two successive Nike shots with similar targets ($\lambda = 30$ μm, $\eta_0 = 6$ μm, 100 μm thickness), differing by the laser pulse shapes and peak amplitudes. The first shot was taken with a short pulse (450±50 ps FWHM centered at $t = 0$, peak intensity 2.1×10^{14} W/cm^2), the next one – with a standard 4 ns Nike pulse as in [8, 13, 14], peak intensity 9.0×10^{13} W/cm^2. In the latter case, the target does not start to accelerate until the end of the laser pulse, so the observed evolution represents the ablative RM oscillation described in detail in [7-10, 14-16]. The single observed late-time phase reversal of δm occurs when the phase of the ripple pattern at the ablation front is changed.

Now consider the former, short-pulse case. While the laser pulse is still on, we observe the same ablative RM oscillation: the early growth of δm, caused mainly by the

straightening of the shock front propagating into the target, as explained in [15, 16], is followed by a decrease due to the onset of the oscillation at the ablation front. Then, at $t \approx 0.25$ ns, the laser pulse ends and the ablation front disappears.

The oscillations continue to proceed in the whole shocked volume of the target. The largest (and comparable) contributions to δm are provided by the oscillating unsupported shock wave propagating into unperturbed material and by the portion of the expansion wave immediately following the shock (see [18]). The high-frequency oscillations of the "short pulse" line in Fig. 2 are essentially standing sound waves. However, rather than propagating on a uniform background, they are superimposed upon the unsteady longitudinal flow caused by the "impulsive loading" of the target [28], which has much in common with a planar blast wave flow [23, 29].

In agreement with the predictions of [18], these oscillations are seen to be very strong compared to the rapidly decaying oscillations of a supported rippled shock wave. Consequently, numerous phase reversals of δm are observable, up to four (with the second harmonic observable near the minima of the first harmonic) as in Fig. 2, where they are marked by vertical arrows. The visible-light streak camera looking at the rear surface detected the shock breakout at $t = 1.74$ ns. The lateral pressure gradient does not disappear together with the shock wave, making one more large-amplitude oscillation possible. Later the free longitudinal expansion reduces the speed of sound in the disintegrating target, freezing the perturbation structure in it: compare the solid and dotted lines in Fig. 1(b).

Figure 3 illustrates the clear observation of three phase reversals of δm in a 125 μm thick target with $\lambda = 45$ μm, $\eta_0 = 6$ μm, irradiated by a 450±50 ps long spike, peak

intensity 1.9×10^{14} W/cm^2. Since the frequency of oscillations of δm scales roughly as c_s / λ, where c_s is the characteristic speed of sound [18, 19], longer ripple wavelength compared to the conditions of Fig. 2 implies that the oscillation frequency here is less by approximately a factor of 1.5, and therefore fewer phase reversals are observed.

Our simulation took into account the plasma radiation, as in Ref. [10]. The simulated shock breakout time is $t = 2.3$ ns, same as observed. Comparing the experimental and simulated time histories of δm shown in the top part of Fig. 3, we find that the FAST2D simulation reproduces both the oscillation frequency and the respective peak amplitudes reasonably well. The first two observed phase reversals occur while the unsupported shock propagates through the unperturbed part of the thick target, and the third one – after the target has started to disintegrate.

The bottom part of Fig. 3 shows that the observed areal mass perturbations δm do not simply pass through several minima but also change phase during each traversal. Indeed, each vertical column of observed horizontal stripes (brighter colors correspond to higher δm) is seen to be shifted with respect to the neighboring column by a half period. Broadband filtering of the streak image in the range of 22 to 50 μm demonstrates the robustness of the observed phase reversals and makes it possible to see the second harmonic modulation emerging near $t = 2$ ns when the dominant mode amplitude is low.

To summarize, we have observed for the first time the strong oscillations of areal mass in a rippled target hit by a strong, short laser pulse. The oscillations occur in an unsupported shock wave that propagates through the target after the end of the laser pulse and is immediately followed by an expansion wave. The observed redistribution of mass proceeds in the volume of the target; the main contribution to δm comes from the

vicinity of the decelerated shock front. The large amplitude and high frequency of these oscillations allowed accurate observations of multiple phase reversals of the areal mass modulation amplitude.

The authors acknowledge the excellent technical support of Nike Laser Crew. This work was supported by the U. S. Department of Energy, Defense Programs.

[1] S. E. Bodner *et al*., *Phys. Plasmas* **5**, 1901 (1998).

[2] V. N. Goncharov *et al*., Phys. Plasmas **10**, 1906 (2003).

[3] R. Betti *et al*., Phys. Plasmas **12**, 042703 (2005).

[4] N. Metzler *et al*., Phys. Plasmas **9**, 5050 (2002); Phys. Plasmas **10**, 1897 (2003).

[5] V. N. Goncharov, Phys. Rev. Lett. **104**, 165001 (2010).

[6] R. Betti *et al*., Phys. Rev. Lett. **98**, 155001 (2007).

[7] V. N. Goncharov, Phys. Rev. Lett. **82**, 2091 (1999).

[8] Y. Aglitskiy *et al*., Phys. Rev. Lett. **87**, 265001 (2001).

[9] O. V. Gotchev *et al*., Phys. Rev. Lett. **96**,115005 (2006).

[10] Y. Aglitskiy *et al*., Phys. Rev. Lett. **103**, 085002 (2009).

[11] R. Betti, V. Lobatchev and R. L. McCrory, Phys. Rev. Lett. **81**, 5560 (1998).

[12] K. Shigemori *et al*., Phys. Rev. Lett. **84**,5331 (2000).

[13] Y. Aglitskiy *et al*., Phys. Rev. Lett. **87**, 265002 (2001).

[14] Y. Aglitskiy *et al*., Phys. Plasmas **9**, 22641 (2002).

[15] V. N. Goncharov *et al*., Phys. Plasmas **13**, 012702 (2006).

[16] Y. Aglitskiy *et al*., Phil. Trans. Roy. Soc. A **368**, 1739 (2010).

[17] A. Marocchino, S. Atzeni, and A. Schiavi, Phys. Plasmas **17**, 112703 (2010).

[18] A. L. Velikovich *et al*., Phys. Plasmas **10**, 3270 (2003).

[19] A. L. Velikovich *et al*., Phys. Plasmas **8**, 592 (2001); Phys. Rev. E **72**, 046306 (2005).

[20] A. J. Schmitt *et al*., Phys. Plasmas **11**, 2716 (2004); N. Metzler *et al*., Phys. Plasmas **6**, 3283 (1999).

[21] Y. Aglitskiy *et al*., Phys. Plasmas **13**, 080703 (2006).

[22] J. H. Gardner *et al*., Phys. Plasmas **5**, 1935 (1998).

[23] R. M. More *et al*., Phys. Fluids **31**, 3059 (1988).

[24] D. Ryu and E. T. Vishniac, Astrophys. J. **313**, 820 (1987); C. Cavet *et al*., in *SF2A-2009: Proceedings of the Annual meeting of the French Society of Astronomy and Astrophysics*, held 29 June - 4 July 2009 in Besançon, France. Eds.: M. Heydari-Malayeri, C. Reylé and R. Samadi, p. 263.

[25] R. Ishizaki and K. Nishihara, Phys. Rev. Lett. **78**, 1920 (1997).

[26] J. L. Weaver *et al*., Phys. Plasmas **14**, 056316 (2007).

[27] Y. Aglitskiy *et al*., Applied Optics **37**, 5253 (1998).

[28] Ya. B. Zel'dovich and Yu. P. Raizer, *Physics of Shock Waves and High-Temperature Hydrodynamic Phenomena* (Dover, New York, 2002), Chapter XII, Section 4; W. Häfele, Z. Naturforsch. A **10a**, 1006 (1955); V. B. Adamskii, Sov. Phys. Acoust. **2**, 1 (1956); A. I. Zhukov and Ya. M. Kazhdan, *ibid.* **2**, 375 (1956).

[29] L. I. Sedov, *Similarity and Dimensional Methods in Mechanics* (Academic, New York, 1959), Chapter IV.

Figure captions

Figure 1 (color on line). (a) Simulated idealized laser pulse waveform and time history of decaying shock wave propagation. (b) Simulated time histories of peak-to-valley areal mass modulation amplitude for target thickness of 53 and 100 μm. (c) Pressure maps shown for the 100 μm target at the instants marked by the circles in (b). The arrows show the prevailing direction of the lateral pressure gradient.

Figure 2 (color on line). Observed time histories of the dominant peak-to-valley Fourier amplitude of the areal mass modulation $|\delta m|$ produced by short and long Nike pulses in thick targets with $\lambda = 30$ μm. The multiple phase reversals of δm in the former case are marked by vertical arrows. The single phase reversal observed in the latter case is marked by an oblique arrow.

Figure 3 (color on line). Top: experimental (solid) and simulated (dotted line) time histories of the dominant peak-to-valley Fourier amplitude of areal mass modulation in a thick target with $\lambda = 45$ μm. Bottom: areal mass perturbations in the range of 22 to 50 μm obtained from the streak image.

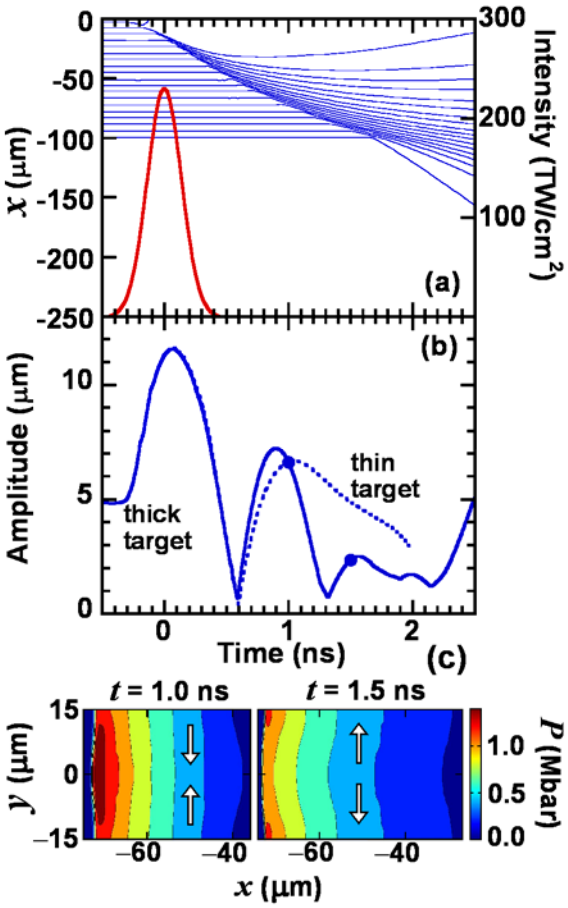

Figure 1 (color on line). (a) Simulated idealized laser pulse waveform and time history of decaying shock wave propagation. (b) Simulated time histories of peak-to-valley areal mass modulation amplitude for target thickness of 53 and 100 μm. (c) Pressure maps shown for the 100 μm target at the instants marked by the circles in (b). The arrows show the prevailing direction of the lateral pressure gradient.

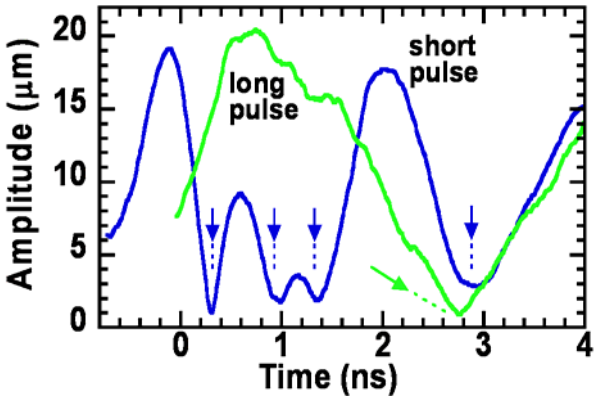

Figure 2 (color on line). Observed time histories of the dominant peak-to-valley Fourier amplitude of the areal mass modulation $|\delta m|$ produced by short and long Nike pulses in thick targets with $\lambda = 30$ μm. The multiple phase reversals of δm in the former case are marked by vertical arrows. The single phase reversal observed in the latter case is marked by an oblique arrow.

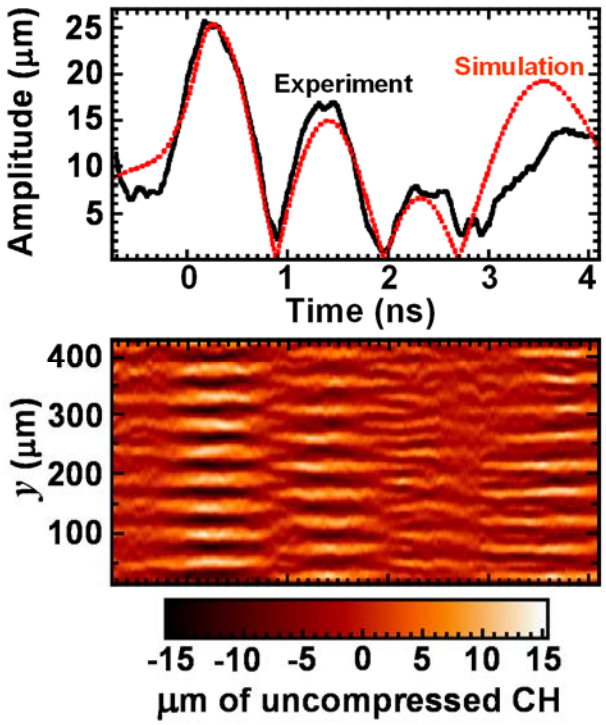

Figure 3 (color on line). Top: experimental (solid) and simulated (dotted line) time histories of the dominant peak-to-valley Fourier amplitude of areal mass modulation in a thick target with $\lambda = 45$ μm. Bottom: areal mass perturbations in the range of 22 to 50 μm obtained from the streak image.